Human Molecular Genetics, 2011, Vol. 20, No. 11 **2116–2130**
doi:10.1093/hmg/ddr094
Advance Access published on March 5, 2011

PRPF mutations are associated with generalized defects in spliceosome formation and pre-mRNA splicing in patients with retinitis pigmentosa

Goranka Tanackovic[1], Adriana Ransijn[1], Philippe Thibault[2], Sherif Abou Elela[2,3], Roscoe Klinck[2], Eliot L. Berson[4], Benoit Chabot[2,3] and Carlo Rivolta[1,*]

[1]Department of Medical Genetics, University of Lausanne, Lausanne 1005, Switzerland, [2]Laboratoire de génomique fonctionnelle de l'Université de Sherbrooke, Sherbrooke, Canada, [3]Département de microbiologie et d'infectiologie, Faculté de médecine et des sciences de la santé, Université de Sherbrooke, Sherbrooke, QC, Canada J1H 5N4 and [4]The Berman-Gund Laboratory for the Study of Retinal Degenerations, Harvard Medical School, Massachusetts Eye and Ear Infirmary, Boston, MA 02114, USA

Received January 10, 2011; Revised February 8, 2011; Accepted March 1, 2011

Proteins PRPF31, PRPF3 and PRPF8 (RP-PRPFs) are ubiquitously expressed components of the spliceosome, a macromolecular complex that processes nearly all pre-mRNAs. Although these spliceosomal proteins are conserved in eukaryotes and are essential for survival, heterozygous mutations in human *RP-PRPF* genes lead to retinitis pigmentosa, a hereditary disease restricted to the eye. Using cells from patients with 10 different mutations, we show that all clinically relevant *RP-PRPF* defects affect the stoichiometry of spliceosomal small nuclear RNAs (snRNAs), the protein composition of tri-small nuclear ribonucleoproteins and the kinetics of spliceosome assembly. These mutations cause inefficient splicing *in vitro* and affect constitutive splicing *ex-vivo* by impairing the removal of at least 9% of endogenously expressed introns. Alternative splicing choices are also affected when RP-PRPF defects are present. Furthermore, we show that the steady-state levels of snRNAs and processed pre-mRNAs are highest in the retina, indicating a particularly elevated splicing activity. Our results suggest a role for *PRPFs* defects in the etiology of PRPF-linked retinitis pigmentosa, which appears to be a truly systemic splicing disease. Although these mutations cause widespread and important splicing defects, they are likely tolerated by the majority of human tissues but are critical for retinal cell survival.

INTRODUCTION

Heterozygous mutations in genes *PRPF31* (RP11, OMIM 606419), *PRPF8* (RP13, OMIM 600059) and *PRPF3* (RP18, OMIM 601414) cause retinitis pigmentosa (RP, OMIM 268000) (1–3), a group of hereditary disorders characterized by progressive degeneration of the photoreceptors, the light-sensing cells in the retina (4).

All of these genes, as well as RP genes *SNRNP200* and *RP9* (5–8), are involved in pre-mRNA splicing, a process by which introns are removed from pre-mRNA and exons are joined to produce mature mRNA. Pre-mRNA processing resulting in a single form of mRNA is defined as constitutive splicing. Conversely, alternative splicing (AS) yields multiple mature transcripts from the same pre-mRNA. In humans, AS is a major contributor to increased protein diversity since >90% of primary transcripts are alternatively spliced (9,10).

Splicing is performed by the spliceosome, a macromolecular complex that contains five uridine-rich small nuclear RNAs (U snRNAs) and over 100 proteins (reviewed in 11). These snRNAs associate with specific proteins to form small nuclear ribonucleoproteins (snRNPs). The U1, U2, U4 and U6 snRNP compose the major (U2-type) spliceosome, processing >99% of all introns, whereas their functional analogs U11, U12, U4*atac* and U6*atac* snRNP, respectively, form the minor (U12-type) spliceosome. U5 snRNP is present in both complexes (reviewed in 11,12).

*To whom correspondence should be addressed at: Department of Medical Genetics, University of Lausanne, Rue du Bugnon 27, Lausanne 1005, Switzerland. Tel: +41 216925451; Fax: +41 216925455; Email: carlo.rivolta@unil.ch

The spliceosome recognizes primarily conserved sequences at intron boundaries: the 5′-splice site (ss), the 3′-ss, the branch-point sequence (BPS) and the poly-pyrimidine tract (poly-Py) (reviewed in 11). *In vitro*, and possibly *in vivo*, the spliceosome assembles on these signals in a step-wise manner, through the following different complexes: E, A, B, B* and C (Supplementary Material, Fig. S1) (reviewed in 11). Joining of the U4/U6.U5 snRNP particle (the tri-snRNP) to complex A (prespliceosome) leads to its conversion into the precatalytic complex B. Major compositional and conformational rearrangements are needed for the catalytic activation of the spliceosome. These involve the release of U1 and U4 snRNPs together with U4/U6 snRNP-associated proteins, following U4/U6 unwinding. These changes result in the formation of complex B* (activated spliceosome), which undergoes the first step of splicing to generate the catalytic complex C. The latter complex is then further rearranged to allow the second catalytic step to occur. Once pre-mRNA splicing is completed, the spliceosome disassembles, U snRNPs are recycled for additional rounds of splicing and the mRNA is released as an mRNP (reviewed in 11).

The RP-related splicing proteins have been proved to be part of the tri-snRNP (Supplementary Material, Fig. S1) (13,14), a particle essential for the major and minor spliceosomes (8,15,16). However, the precise mechanism by which defects in these essential spliceosome components result in RP has so far remained obscure.

In this work, we analyze the function and the composition of spliceosomes in human cells with *PRPF31*, *PRPF3* and *PRPF8* mutations and propose a model linking generalized pre-mRNA splicing deficiency and hereditary retinal degeneration. Since PRPF animal models have so far failed to provide conclusive answers (17–19) and since retinal biopsies to examine photoreceptors directly are not an ethically sustainable option, we took advantage of the widespread expression of these splicing factors and the common function of the spliceosome across tissues to perform *in vitro* and *ex vivo* studies in lymphoblasts from patients with 10 different mutations in all three *RP-PRPF* genes. Using this approach, we document that mutations in *RP-PRPF* genes alter the levels of snRNAs and cause defects in generic and AS. Our findings therefore reveal that RP-PRPF genes can selectively affect splicing decisions and indicate that RP may be a splicing disease to which retinal cells are most sensitive.

RESULTS

Retina expresses the highest amount of spliceosomal snRNAs and processes the largest volume of pre-mRNAs

We quantified snRNAs in a panel of five human tissues (including retina) and two cell lines. Our results, normalized to 18S and 28S rRNAs, showed that retina expressed approximately seven times more major snRNAs than the other tissues tested and approximately two times more of these molecules than highly proliferative human cell lines (Fig. 1A). In addition, it expressed roughly twice as many minor snRNAs when compared with the other samples, with the exception of testis, which displayed comparable amounts (Fig. 1B).

To test whether the high level of snRNAs in retina was related to the volume of pre-mRNA splicing, we computed the amounts of 2255 processed housekeeping transcripts (Supplementary Material, Table S1) across 31 human tissues using available expression microarray data (20). We found that retina produced the highest amounts of spliced transcripts (Fig. 1C).

Although these data were obtained by completely unrelated procedures and on different primary samples, the levels of major spliceosome snRNAs and of spliced housekeeping genes (containing mostly U2-type introns) correlated very well across tissues (compare Fig. 1A and C).

RP-PRPF mutations

We obtained lymphoblast cell lines from 13 patients belonging to families with dominant RP and with distinct mutations in *RP-PRPF* genes (Supplementary Material, Table S2). In all downstream experiments, data were obtained for at least two independent mutations per *RP-PRPF* gene and for two distinct controls. Whenever the results were identical for different mutations within the same gene, representative results for one of them are shown.

Altered snRNP levels and relative composition of the tri-snRNP in cells with mutations in *PRPF31*, *PRPF3* or *PRPF8*

To detect any abnormalities in the migration and composition of spliceosome components, we fractionated nuclear extracts from cell lines of patients with RP-PRPF mutations (Supplementary Material, Table S2) in 10–30% glycerol gradients. snRNAs from the major and the minor spliceosomes were visualized by northern blotting and their relative amounts determined by densitometry (Fig. 2). Comparison of nuclear extracts from control lymphoblasts and HeLa cells showed that all snRNAs studied had the same distribution across the gradient (Fig. 2 and data not shown). The fractionation of RP-PRPF extracts revealed a distribution of snRNAs that was comparable with controls (Fig. 2A) and indicated that snRNPs had similar molecular weights. Nevertheless, by quantitative assessment of snRNA amounts (normalized to U1 snRNA), we found that U2 snRNA was reduced by ∼13–18% in all RP-PRPF extracts relative to the controls (Fig. 2C). The amounts of snRNAs composing tri-snRNPs were even more reduced in these extracts: RP-PRPF extracts had ∼63–76% of U4 snRNA, ∼52–63% of U5 snRNA and ∼53–74% of U6 snRNA (Fig. 2C). The amounts of minor snRNAs did not appear to be globally affected in RP-PRPF cells, with the exception of U4*atac* and U6*atac* in cells with *PRPF8* mutations (Fig. 2C), where they were reduced by 20 and 44%, respectively, compared with controls. We also assessed the distribution of a subset of tri-snRNP proteins by fractionation in glycerol gradients (Fig. 2B) or by immunoprecipitation from total extracts (Supplementary Material, Fig. S2). In all extracts tested, tri-snRNP components accumulated in fractions 18–21 of the gradient (Fig. 2).

In cells with *PRPF31* mutations, glycerol gradient revealed no qualitative change in the distribution of the tested tri-snRNP proteins (Fig. 2B). The immunoprecipitation

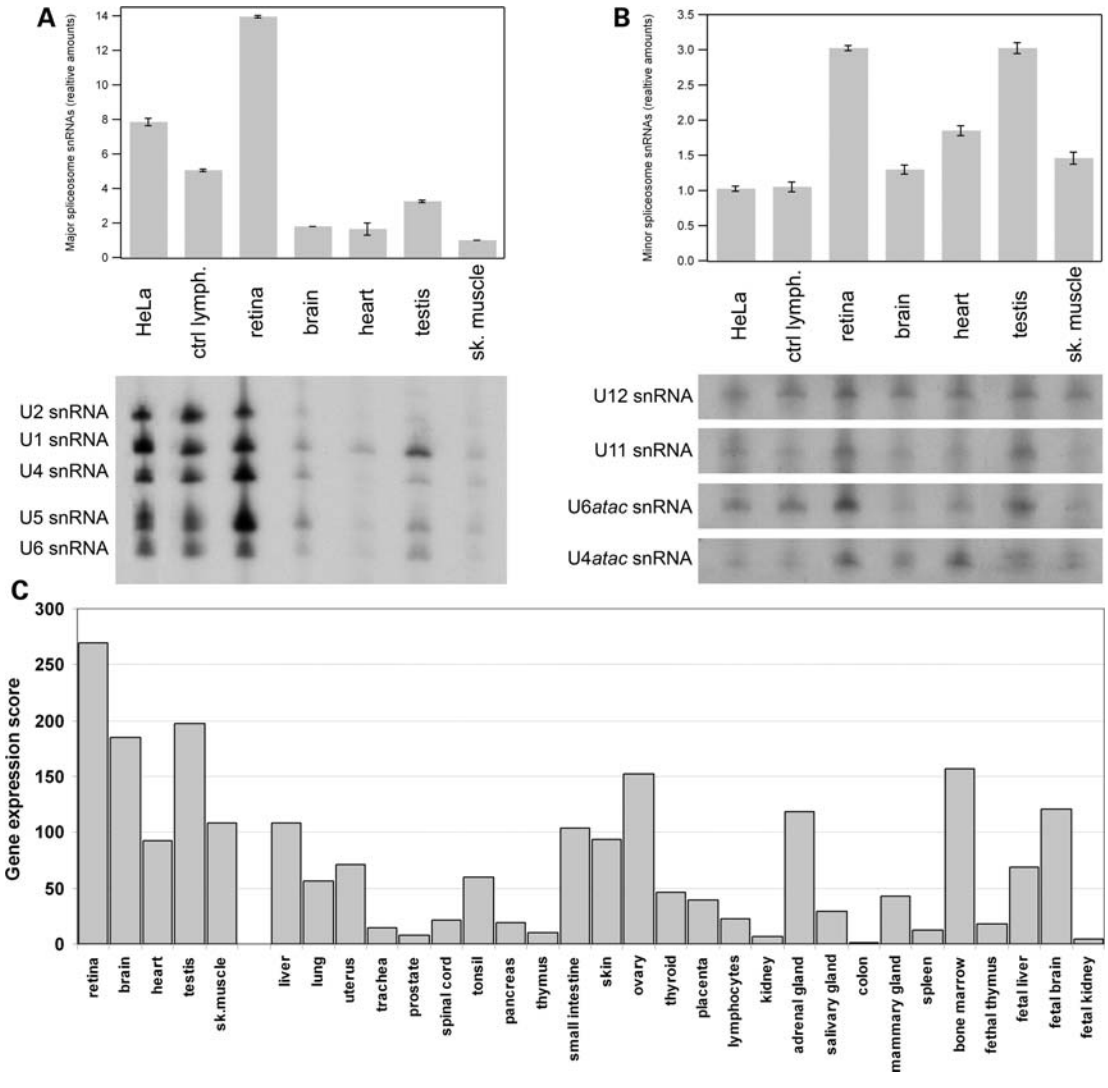

Figure 1. Human retina expresses more snRNAs and processes the highest amounts of housekeeping transcripts. Relative amounts of snRNAs in various tissues, as assessed by northern blotting with probes against major (**A**, bottom) or minor (**B**, bottom) spliceosomal snRNAs, are shown. Densitometry analyses are provided on the top panels. (**C**) Evaluation of the expression of 2255 housekeeping genes across 31 human tissues revealed that retina produces the highest amount of constitutive mRNAs. The 'gene expression score' indicates the number of instances for which a given gene was maximally expressed in a tissue.

showed, however, that all tri-snRNP proteins tested were present at ∼60% with respect to controls (Supplementary Material, Fig. S2). Since this deficit was not due to their overall reduced availability in the cells (Supplementary Material, Fig. S3), our data suggest that lymphoblasts with *PRPF31* mutations correctly assembled tri-snRNPs, but in a less efficient manner compared with controls. However, this phenomenon was not immediately visible in glycerol gradient experiments, probably because of the lower sensitivity of the western procedure to detect small amounts of proteins present in individual fractions.

In cells with *PRPF3* mutations, PRPF3 accumulated in fractions containing tri-snRNPs and was absent elsewhere, indicating that mutant PRPF3 proteins stably associated with tri-snRNPs (Fig. 2B). In contrast to the other tri-snRNP proteins tested, PRPF4, hBrr2 and hSnu114 showed an altered distribution, as they were also present in the lower molecular weight fractions (Fig. 2B). Quantification of immunoprecipitated tri-snRNP proteins showed that only ∼50% of PRPF4 was associated with snRNPs, compared with the control (Supplementary Material, Fig. S2). Similarly, hBrr2 and hSnu114 proteins were also present in reduced amounts (∼30% and ∼50%, respectively, Supplementary Material, Fig. S2).

Glycerol gradient analysis of RP-PRPF8 extracts showed an absence of PRPF8 in fractions lighter than those specific to U5 or the tri-snRNP (Fig. 2B), suggesting that both wild-type and mutant proteins are present in U5 and the tri-snRNPs. Notably, hBrr2, hSnu114 and PRPF6 displayed an altered distribution (in addition to their presence in fractions 18–21), likely indicating an impaired interaction with mutant PRPF8. Immunoprecipitation showed that, relative to the control, only ∼10% of hBrr2, ∼50% of hSnu114 and ∼80% of PRPF6 were associated with the snRNPs (Supplementary Material, Fig. S2).

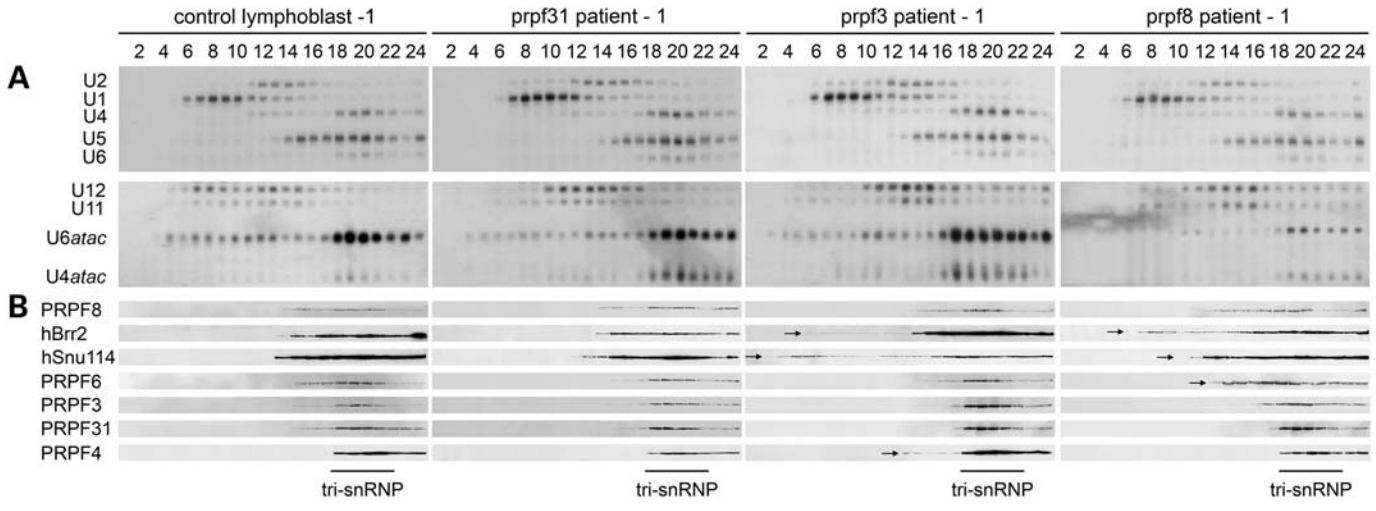

C

U1	1.00	1.00	1.00	1.00
U2	0.55±0.14 (1.00)	0.46±0.10 (0.85)	0.47±0.11 (0.87)	0.44±0.12 (0.82)
U4	0.69±0.05 (1.00)	0.52±0.06 (0.76)	0.43±0.06 (0.63)	0.52±0.05 (0.76)
U5	1.47±0.01 (1.00)	0.92±0.03 (0.63)	0.76±0.02 (0.52)	0.89±0.03 (0.61)
U6	0.31±0.09 (1.00)	0.23±0.08 (0.74)	0.16±0.06 (0.53)	0.17±0.06 (0.57)
U11	1.00	1.00	1.00	1.00
U12	1.09±0.09 (1.00)	1.18±0.10 (1.08)	1.13±0.01 (1.04)	1.06±0.06 (0.97)
U4*atac*	1.02±0.04 (1.00)	1.09±0.01 (1.07)	1.20±0.08 (1.17)	0.81±0.01 (0.79)
U6*atac*	1.83±0.30 (1.00)	1.82±0.26 (1.00)	1.88±0.15 (1.03)	1.03±0.01 (0.56)

Figure 2. Glycerol gradient fractionation reveals alterations of tri-snRNP composition in RP-PRPF lymphoblasts. Nuclear extracts from control or patient lymphoblasts, as indicated on the top of the figure, were fractionated in parallel on 10–30% glycerol gradients. Fractions were collected from the top to the bottom of the gradient and processed as follows. (**A**) RNA was extracted and analyzed by northern blotting. Identities of detected snRNAs are shown on the left. (**B**) Proteins (indicated on the left) present in each fraction were visualized by western blotting. The tri-snRNP-containing fractions are indicated on the bottom of the panel (solid, horizontal bars). Arrows indicate tri-snRNP proteins abnormally distributed across the gradient, with respect to the control. (**C**) Densitometry measurements of northern blots were normalized to the measured U1 snRNA amounts. Quantity of the each snRNA is expressed as a ratio to the corresponding snRNA in control lymphoblasts (average ± standard deviation) and as percent of control values, in parentheses.

Spliceosome assembly is delayed in extracts from patient cell lines

Altered levels of snRNAs suggest that some aspects of spliceosome formation and function may be affected. To investigate this possibility, we assessed *in vitro* spliceosome assembly in nuclear extracts from lymphoblasts by using *RNA1*, a model pre-mRNA that contains all necessary splicing signals (21) (Supplementary Material, Fig. S4A). Extracts from control lymphoblasts followed the same kinetics of spliceosome assembly as HeLa extracts, which are commonly used in this type of assay (Fig. 3A). Conversely, extracts from lymphoblasts with *RP-PRPF* mutations showed slower kinetics of complex A accumulation, with maximal level of assemblies appearing later than in controls (Fig. 3A, arrows). In addition, formation of complexes B and C was inefficient; catalytic complex C is normally visible after 30 min in control reactions, but was barely detected in extracts from patients even after 120 min (Fig. 3A). Our results indicate that nuclear extracts from patient cells can form spliceosomes *in vitro*, although the process has reduced kinetics.

The observed delay in complex A accumulation may be direct or caused by its altered conversion into downstream structures. To distinguish between these possibilities, we assembled splicing complexes using a mutant *RNA1* lacking the 5′-ss (Supplementary Material, Fig. S4B), and onto which spliceosome assembly is blocked at the level of complex A (22). As shown in Figure 3B, all extracts reached the peak level of complex A at 15 min, suggesting that the delay in spliceosome formation in cells with RP-PRPF defects is due to a defect occurring after complex A. The above observations suggest that conversion of complex A into complex B is defective in RP-PRPF cells and that this defect impacts the kinetics of accumulation of complex A and the efficiency of all subsequent tri-snRNP-dependent steps.

Pre-mRNA splicing is affected in lymphoblasts carrying RP-PRPF mutations

To assess whether defects in spliceosome composition and assembly affect processing of pre-mRNA, we performed *in vitro* splicing assays using *RNA1* as substrate. Although all nuclear extracts tested could splice this pre-mRNA, samples from patient lymphoblasts showed a reduced splicing efficiency (Fig. 4).

Because of the splicing defect observed *in vitro*, we then tested splicing of endogenously expressed transcripts in lymphoblast cells by reverse transcription polymerase chain reaction (RT-PCR) using primers that allowed the simultaneous amplification of both spliced and unspliced products. Since mammalian splicing signals are degenerate, we selected a

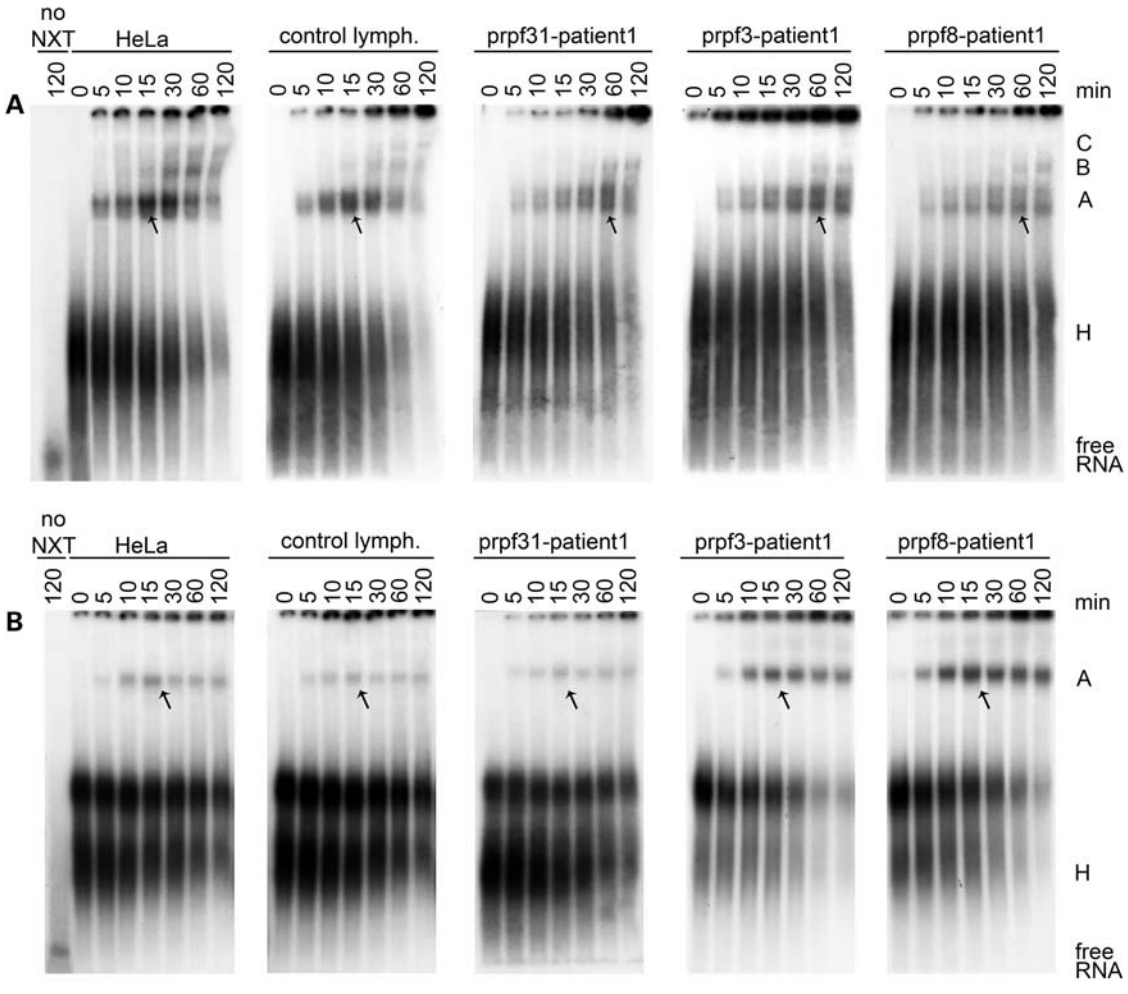

Figure 3. Kinetics of spliceosome assembly is delayed in cell lines from patients with *RP-PRPF* mutations. Nuclear extracts from HeLa and lymphoblast cells, as indicated on top of the panels, were mixed with *in vitro*-transcribed radiolabeled *RNA1* RNA (**A**) or its mutant version lacking the 5′-ss (**B**) and incubated under splicing conditions. At indicated time points, the reactions were stopped, and complexes resolved by native 4% (A) or 5% (B) PAGE and visualized by autoradiography. Identity of the spliceosome complexes A–C and the free RNA is indicated on the right. Complex H is formed upon binding of hnRNP proteins to RNA and is not specific to the spliceosome. Arrows show the maximal amount of complex A in each assay.

panel of 57 introns recapitulating typical sequence motifs found in the human genome, including targets for U2 and U12 spliceosomes (Supplementary Material, Table S3). Furthermore, for each intron type, we scored conservation of different splicing elements. Although none of the introns tested belonged to specific RP genes, they carried splicing signals that are present in such genes. As many as 5 out of 57 splicing units (8.8%) accumulated unspliced products in cells from patients with *RP-PRPF* mutations (Fig. 5). For two of these, we observed a gene-specific splicing defect (i.e. intron 8 of *MATN4* and intron 1 of *CBLN1*). However, this effect was not (within the same *PRPF* gene) mutation specific and seemed not to depend on the type of intron tested (Supplementary Material, Fig. S5).

Alternative splicing is affected in *RP-PRPF* cells

Splice site selection often relies on kinetic choices. The slowdown of specific tri-snRNP-dependent steps of spliceosome assembly on competing pairs of splice sites may favor the use of one combination over another; likewise, a change in the stoichiometry of snRNAs may also influence the choice of alternative splice sites (23). We investigated whether AS could be affected in RP-PRPF cells. We therefore analyzed the splicing pattern in 13 cell lines with *RP-PRPF* mutations and 11 control lymphoblasts using a RT–PCR platform that interrogated 96 alternative splicing events (ASEs). Each test was designed to detect a long and a short isoform. For each ASE, we computed its specific percentage of splicing index (PSI), defined as the ratio between the long isoform over the sum of the short and long isoforms. When more than two products were observed, the short and long products were selected to maximize their total abundance across the reaction set.

Considering a false discovery rate of 0.15, three significant scores were obtained for cell lines bearing *PRPF31* mutations for genes *AXIN1*, *BCL2L11* and *HSC20* (Fig. 6A; all splicing profiles and electropherograms can be consulted on http://palace.lgfus.ca). The analysis of the four RP-PRPF8 and three RP-PRPF3 cell lines yielded no ASEs harboring

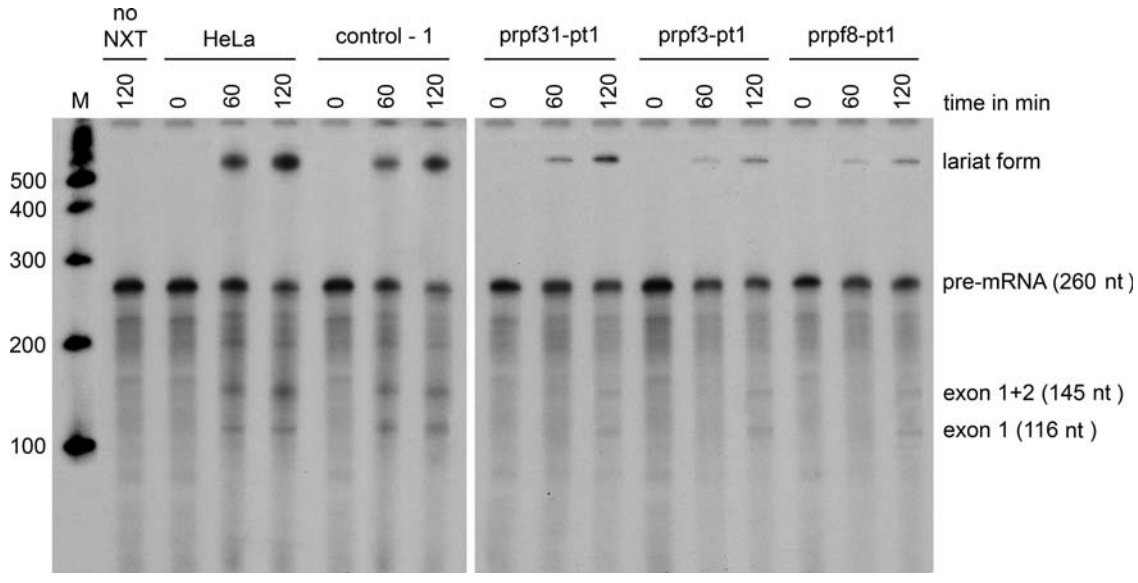

Figure 4. *In vitro* pre-mRNA splicing is less efficient in extracts from patients with RP. Nuclear extracts from HeLa and lymphoblast cells, as indicated on the top (pt, patient), were used in *in vitro* splicing assays with radiolabeled *RNA1* RNA as substrate. At indicated time points, RNA was extracted from the reactions, separated by 8% polyacrilamide/8.3 M urea gels and visualized by autoradiography. Migration of pre-mRNA and of its splicing products is indicated on the right. The radiolabeled molecular weight marker (M, in nt) is shown on the left. no NXT: no nuclear extract.

significant *q*-values. However, the limited number of available (different) cell lines for these two latter RP-PRPFs would not allow a confident detection of significant events, unless these caused very large effects.

Since mutated RP-PRPF proteins may promote aberrant splicing and produce novel splice isoforms, we inspected our data for the occurrence of novel RT–PCR products that might be associated with these conditions. With the caveat that none of these products has been confirmed to be a mis-splicing event, we noted that the RT–PCR product at 175 bp for the *APP* transcript was strikingly more prevalent in RP-PRPF31 samples than in controls and other RP-PRPF samples (Fig. 6B). The 379 bp product for *FGFR1* was detected only in three cell lines with *PRPF31* mutations but never in controls or other RP-PRPF cell lines (Fig. 6C). The 665 bp and 793 bp products of *TNFRSF10B* (also known as *TRAIL-R2*) were detected in most cells with *RP-PRPF* defects and never in controls (Fig. 6D). While the 337 bp product of *BMP4* was less abundant in most samples with *PRPF31* and *PRPF8* mutations, the 195 bp product showed opposite behavior (Fig. 6E). Finally, the 378 bp product for *UTRN* was detected only in RP-PRPF31 and RP-PRPF8 cell lines, but not in the other samples (Fig. 6F).

Depleting PRPF8 in human cell lines alters alternative splicing

All RP-PRPF cell lines analyzed were derived from patients with heterozygous mutations, hence always bearing a wild-type allele expressing a functional protein product. For this reason, the biological defects detected in cells from patients with naturally occurring mutations may be subtle and/or obscured by the activity of this functional allele. To circumvent this masking effect, we stressed the experimental system by provoking a stronger *RP-PRPF* deficiency. We chose to deplete PRPF8 by siRNA, since this protein has been shown to play a central role in the splicing process (24) and, unlike PRPF31 and PRPF3, it is present during the catalytic steps of intron excision.

The same set of 96 previously described ASEs was analyzed following PRPF8 depletion in five cell lines: MCF-7, MDA-MB-231, PC-3, OVCAR-3 and SKOV3. Depletion efficiencies were determined using quantitative PCR (qPCR) and were considered adequate only if the depletion was superior to 50%. For tests satisfying this condition, a $\triangle$PSI value, defined as $PSI_{knockdown} - PSI_{control}$, was computed. From over 1000 $\triangle$PSI values collected, nearly one-tenth had values greater than 10 percentage points with both siRNAs when all five cell lines were considered (Table 1). A 10% change in PSI provides a Z-score above 1.5, which represents 1.5 standard deviations above or below the average variation observed for thousands of controls performed for all splicing units in these cell lines (25). The proportion of units that shifted upon depleting PRPF8 ranged from $\sim$10% for MCF-7 cells to nearly 30% for SKOV3, but such variations may be due to the depletion efficiencies. The hit overlap across all cell lines was considerable, with over half (26/49) of the shifted ASEs occurring in two or more cell lines. Eight units (*APG5L*, *DDR1*, *F3*, *FANCA*, *PPP3CB*, *PTPN13*, *SHMT1* and *TNFSFR10B*) reacted similarly to PRPF8 depletion in at least four of the five cell lines. These results demonstrate that reducing the level of PRPF8 in mammalian cells can alter the AS of numerous genes, and that a substantial fraction of these effects are common to cell lines of different origins.

DISCUSSION

Despite recent fundamental research performed in yeast or standard laboratory cell lines, the molecular link between

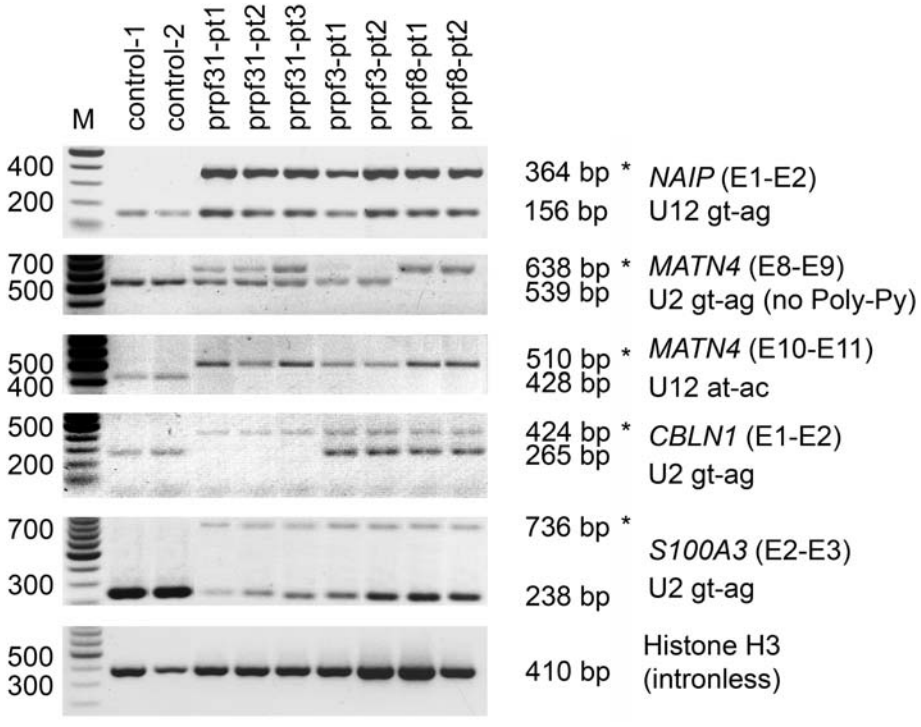

Figure 5. Splicing of a subset of introns is impaired in metabolically active lymphoblasts with *RP-PRPF* mutations. RT–PCRs were performed to analyze constitutive splicing events on transcripts extracted from living lymphoblasts (from controls and patients, 'pt') and bearing a variety of splicing signals. Splicing units that were not correctly spliced are shown. Histone H3 is a positive amplification control. Identity and sizes of the PCR products are indicated on the right of the figure. Exons containing the PCR primers are indicated by 'E#'. Migration of unspliced RT–PCR products is indicated by asterisks. Sizes of the molecular weight markers (M, in bp) are indicated on the left.

RP-PRPF proteins and the pathogenesis of retinitis pigmentosa has not been fully clarified. By quantification of major and minor snRNAs, we unexpectedly found that the retina normally expresses up to 7-fold more major snRNAs and approximately twice as many of the minor snRNAs compared with other human tissues. The higher level of snRNAs in the retina is a likely consequence of another surprising result; i.e. this tissue contains the highest volume of processed pre-mRNAs within the whole body, as measured by the amount of spliced genes that were common to 31 human tissues. These results suggest that a deficiency in spliceosome components would be more deleterious for the retina than for other human tissues.

To explore the nature of this potential defect leading to RP, we used lymphoblast cell lines derived from patients with RP with 10 different mutations in all 3 *RP-PRPF* genes. Glycerol gradient centrifugation of nuclear extracts revealed alterations in the stoichiometry of the snRNAs, as well as altered tri-snRNP protein composition, in cells carrying *RP-PRPF* mutations. Relative to U1 snRNA, U2 snRNA was reduced by 13–18%, while tri-snRNAs were decreased up to 50%. Minor snRNAs were also decreased but only for U4*atac* and U6*atac* in RP-PRPF8 cells. Quantitative assessment of tri-snRNP protein composition by immunoprecipitation indicated that cells from patients with *PRPF31* mutations assembled roughly half of these particles with respect to controls. These data are in agreement with previous work showing that *PRPF31* alleles causing RP result in short-lived or absent mRNAs and therefore in no mature protein (26–28). Consequently, in these cells, only the wild-type allele can provide functional protein. Although the observed defects are less pronounced compared with complete RNAi-mediated depletion of PRPF31 in HeLa cells (29), they are in agreement with the described essential role of PRPF31 in tri-snRNP assembly and spliceosome formation (29–31).

Unlike defects in the *PRPF31* gene, *PRPF3* and *PRPF8* mutations are predicted to yield stable mutant proteins that are co-expressed in heterozygotes with their wild-type counterparts (2,3). Our results support this idea: comparable amounts of PRPF3 and PRPF8 were identified in nuclear extracts from patient and control lymphoblast cells. In addition, glycerol gradient fractionation and immunoprecipitation experiments showed that both mutant and wild-type PRPF8 and PRPF3 proteins were stably associated with tri-snRNPs in the corresponding cell lines. Tri-snRNPs bearing the PRPF3 and PRPF8 mutant proteins did assemble and had similar molecular weights to those of controls, but contained reduced amounts of hSnu114 and hBrr2. Since the two latter proteins are involved in U4/U6 and U4*atac*/U6*atac* snRNA unwinding (32–35), our results suggest that RP-PRPF3 and RP-PRPF8 mutations could affect this process, necessary for the catalytic activation of the spliceosome. In agreement with our results, it has been demonstrated that the yeast homolog of PRPF8-R2310G (one of the mutant PRPF8 forms analyzed here) impairs U4/U6 snRNA unwinding by Brr2, resulting in the disregulation of catalytic

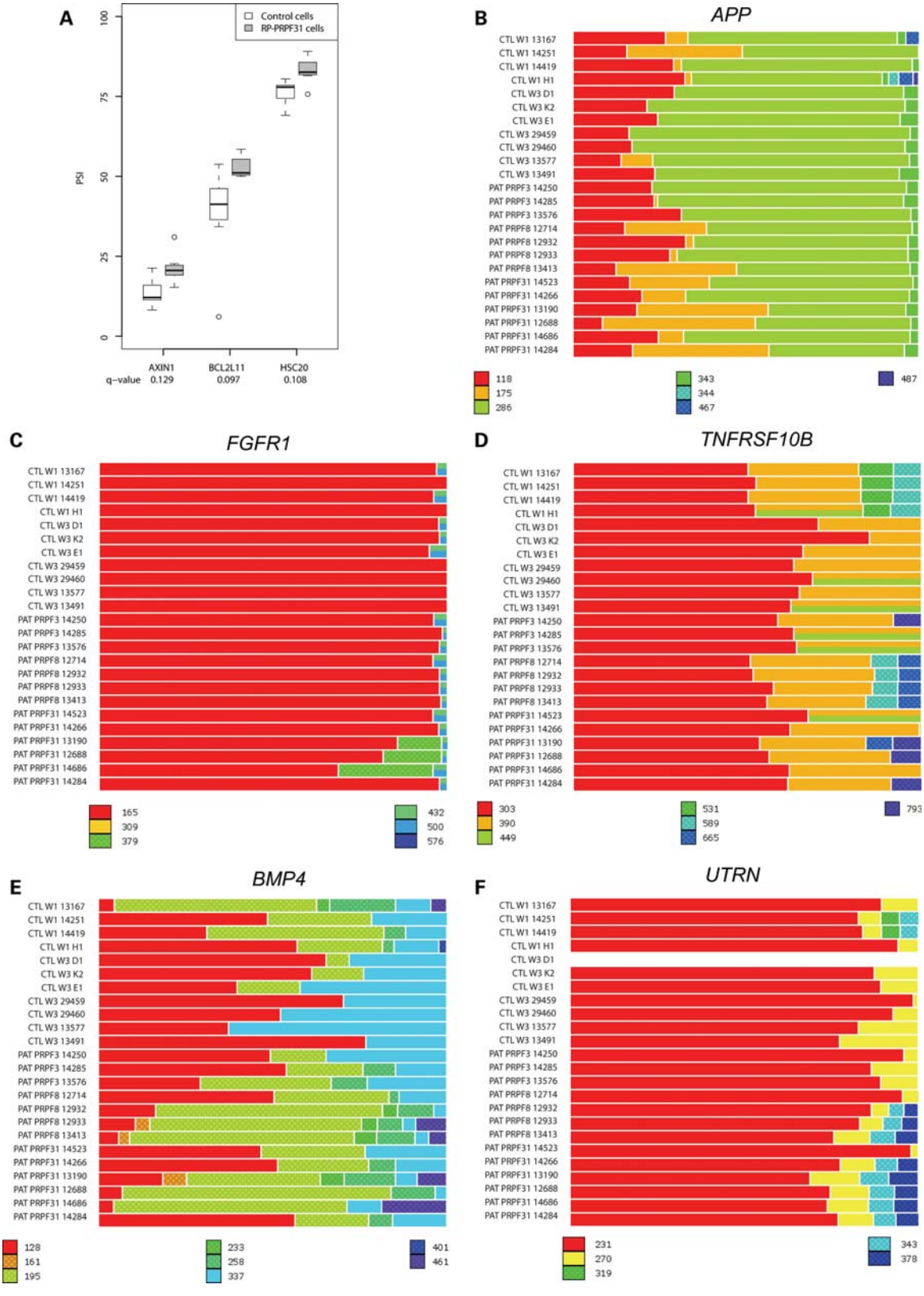

Figure 6. Impact of *PRPF* mutations on the splicing profiles of selected ASEs. (**A**) Three ASEs that reacted to the presence of mutations in *PRPF31*. The boxplots depict inclusion percentage (PSI or percent splicing index) for known alternative exons for individual ASEs. The boxes include values in the first to third quartiles; the thick horizontal line indicates the median; whiskers extend to data points at or less than 1.5 times the interquartile range. Circles are outliers. *q*-values are indicated on the x-axis. (**B**–**F**) Graphical representation of the relative abundance of all RT–PCR products obtained for selected ASEs using lymphoblast cell lines derived from controls or patients with *RP-PRPF* mutations. The size of the products is indicated in the legend (in bp).

Table 1. Impact of PRPF8 on the AS of 96 ASEs

		AKAP13	APAF1	APC	APG5L	APP	AXIN1	AXL	BCAS1	BCL2L1	BTC	C11orf4	C1orf16	CAPN3	CHEK2	DDR1	NALP1	DNMT3B
MCF7	siPRPF8_1	−10.3	−27.2		1.5	−27.1	−3.8		1.2	−8.0		−27.1	10.6			−20.2		−24.9
	siPRPF8_2	−1.7	2.7	−4.6	11.4	3.2	14.3		4.7	0.7	8.4	6.0	−4.8		−15.8	−13.1		−6.3
MDA-MB-231	siPRPF8_1	−15.0	−16.2	−12.5	−20.2	−5.3	7.3	0.8	−30.1	−5.4	−15.6	−25.7	−1.5	4.3	−33.6	−22.4	−18.4	−3.9
	siPRPF8_2	−4.4	−7.0	−8.0	−14.5	−2.9	34.9	12.7		−8.1	−5.7	−25.1	−1.5	0.3	−18.0	−21.2	−18.2	−3.9
OVCAR-3	siPRPF8_2	−20.6	−7.6	−40.0	−17.7	−7.9	8.2	27.5	2.6	−11.2	−4.6	−8.0	−0.6	−18.8	−8.1	−13.1		−13.8
	siPRPF8_1	−31.3	−17.2	−39.6	−18.6	−15.8	6.2	20.1	0.0	−11.8	−12.4	−12.3	−8.9		−7.6	−21.5		−19.3
PC-3	siPRPF8_1 (exp1)	−36.0	−24.0	−22.4	−41.3	−23.1	9.8	−6.9	6.4	−6.4	−28.3	−31.0	−7.5	−24.0	−13.3	−14.9	−20.7	−13.8
	siPRPF8_2 (exp1)	−12.8	−18.6	−24.6	−20.3	−8.8	17.8	9.1	6.4	−5.3	−28.1	−3.1	−8.3	−20.8	−13.2	−0.4	−2.2	−15.8
	siPRPF8_1 (exp2)	−29.0	−38.8	−15.5	−34.1	−26.6	19.5	1.6		−25.3	−18.0	−26.4	0.4	0.0	−25.9	−32.7	−15.0	−2.8
	siPRPF8_2 (exp2)	−9.0	−13.3	−10.0	−23.2	−16.8	24.3	6.7		−24.6	−22.4	−3.2	−2.9	0.0	−23.0	−28.8	−9.2	−5.6
SKOV3	siPRPF8_1	−9.3	−28.0	−47.7	−14.1	−4.1	17.0	2.7	22.7	−19.6	−13.0	−8.1	−10.6	−11.7	−18.8	−24.7	−36.4	−2.9
	siPRPF8_2	−8.0	−29.9	−48.0	−10.4	−2.9	17.2	8.1	18.6	−17.8	−7.8	−7.5	−11.9	−7.9	−14.1	−19.9	−22.7	−2.9

		DRF1	F3	FANCA	FANCL	FGFR1OP	FGFR2	FGFR4	FN1	FN1	FN1	HMGA1	HMMR	HSC20	LGALS9	LIG3	MAPT	MCL1
MCF7	siPRPF8_1	1.6	−5.2	−19.1	4.5	13.2	12.9		2.8	2.3		8.0	−0.4		38.9	19.9	−8.7	−20.5
	siPRPF8_2	9.0	7.0	3.6	33.7	16.3	45.6	29.6	5.1	20.4	18.5	14.1	8.2	−0.2	−4.5	30.3	0.3	7.7
MDA-MB-231	siPRPF8_1	−18.3	−14.7	−10.8	−5.3	15.0		−21.6	1.8	23.3	12.5	9.4	−29.5	−25.5	15.8	−3.2	−20.8	−13.4
	siPRPF8_2	−13.9	−13.7	−15.1	−0.4	12.7			0.4	1.2	14.9	9.9	−12.9	−21.0	−3.2	2.1	−2.0	−5.5
OVCAR-3	siPRPF8_2	−7.6	−12.1	−14.5	11.9	12.0	14.9	−11.0	3.9	−11.0	8.6	10.2	−3.1	−8.9	−1.9	0.9	−2.9	−4.0
	siPRPF8_1	−8.8	−14.9	−25.9	−2.5	15.1	−4.7		1.9	−15.2	17.5	8.3	−11.1	−15.9	4.9	−4.8	−6.7	−5.6
PC-3	siPRPF8_1 (exp1)	−27.5	−12.3	−15.1	−2.4	12.7			10.4	19.7	22.0	11.5	6.4	−13.9	43.9	6.3	−36.3	−17.3
	siPRPF8_2 (exp1)	−12.2	−16.7	−23.1	1.7	2.3		25.7	1.8	−8.1	17.7	17.5	−2.6	−11.2	0.1	2.0	−20.8	−14.0
	siPRPF8_1 (exp2)	−16.1	−27.3	−23.5	5.0	11.7		69.1	8.0	12.9	22.8	13.6	−1.9	−2.5	24.7	−6.8	−15.2	−14.2
	siPRPF8_2 (exp2)	−16.5	−24.4	−37.2	−10.7	9.3		49.1	2.7	−6.9	17.1	15.8	−1.2	−8.1	−2.6	−3.9	−10.2	−14.3
SKOV3	siPRPF8_1	6.5	−35.2	−18.3	10.6	24.7	18.1	29.4	33.2	7.8	31.8	23.8	1.0	−25.4	−17.8	2.6	−3.1	−6.7
	siPRPF8_2	8.6	−35.0	−17.6	12.3	20.9	8.0	15.5	23.1	−5.5	36.1	24.9	3.8	−25.3	−36.7	−2.2	−2.1	−9.6

		PCSK6	POLB	POLI	PPP3CB	PTPN13	PTPRB	RUNX2	SHMT1	SPP1	SYK	SYNE2	TNFRSF10B	TOPBP1	TSSC4
MCF7	siPRPF8_1	−14.6	9.9		−23.1	−8.6		−18.0	−11.1		−28.2	0.0	26.7	13.7	
	siPRPF8_2	−5.7	21.4	0.6	−23.0	−6.1		−11.1	3.3		9.1	3.1	30.9	19.2	17.2
MDA-MB-231	siPRPF8_1		7.2	10.4	−32.0	−30.2	−34.2	−7.3	−18.4	−8.0	−39.0	2.2	34.6	9.7	4.8
	siPRPF8_2	−52.3	11.1	26.8	−32.0	−24.4	2.8	−5.5	−23.1	−11.0	6.1	11.7	38.8	9.4	2.3
OVCAR-3	siPRPF8_2	−12.3	11.1	17.8	−18.7	−13.0	−18.1	−16.0	−10.0	−19.1	−2.6	3.6	22.6	7.9	15.7
	siPRPF8_1	12.8	−0.1	18.5	−18.7	−14.3	−16.1	−13.1	−15.6	0.7	−25.5	−4.4	22.6	2.6	11.8
PC-3	siPRPF8_1 (exp1)		9.9	11.8	−48.6	−33.8	−53.7	−12.3	−6.1		−57.3	−13.3	37.7	−4.1	10.3
	siPRPF8_2 (exp1)	38.3	4.9	6.6	−40.3	−28.0	−36.1	−14.9	−13.3	−20.4	−3.3	33.8	35.8	3.6	1.1
	siPRPF8_1 (exp2)		18.2	8.9	−25.7	−36.4		−3.1	−18.8	−50.3	−50.9	−12.5	41.4	6.9	12.4
	siPRPF8_2 (exp2)		13.5	20.3	−25.6	−34.8		−3.6	−23.8	−22.9	−25.6	32.3	32.6	3.7	7.1
SKOV3	siPRPF8_1	−22.0	−11.7	13.0	−32.4	−18.8	−13.6	−11.8	−17.5	−25.4	−20.3	24.8	47.0	8.7	31.5
	siPRPF8_2	−19.8	−15.6	14.1	−32.3	−15.6	−4.5	−15.3	−18.9	−18.0	−9.4	33.3	44.6	8.8	29.5

The table only lists ASEs that reacted to the depletion of PRPF8 in at least one of the cell lines tested. ΔPSI values are given for each of the two siRNAs tested. Empty squares with no value indicate that no products were detected. The experiment on PC-3 cells was repeated on a different day and yielded very good reproducibility (Pearson's correlation coefficients of 0.867 and 0.830 for si1 and si2, respectively). Dark gray squares indicate that all samples from a given cell line (or at least three out of four for PC-3) yielded a change superior to 10% relative to controls done on the same day. To access all the data of the experiment, go to http://palace.lgfus.ca/ to obtain an interactive version displaying the compilation and individual electropherograms.

activation of the spliceosome (36). Impairment of the tri-snRNP assembly has been observed by Boon *et al*. (37) in a yeast strain carrying the same mutation. The observed alterations in the stoichiometry of U4, U5 and U6 snRNAs in human cells with PRPF8-R2310G could indicate that a similar dysfunction may also be happening in these cells, although at steady-state we observe most of the U4 and U6 (or their minor spliceosome counterparts) in the tri-snRNP-containing portions of the gradient.

Tri-snRNPs containing mutant PRPF3 proteins are also partially devoid of PRPF4 (~50%), whereas those containing mutant PRPF8 partially lack PRPF6 (~75%). Both PRPF4 and PRPF6 play a role in the tri-snRNP assembly (29,31,38,39) and have been shown to have an additional role in the catalytic activation of the spliceosome (14,40–42).

To investigate whether alterations in the stoichiometry of spliceosome components elicited defects in its formation, we performed *in vitro* assembly assays. Our analysis in nuclear extracts from patient lymphoblasts showed a substantial delay in the formation of the splicing complex A. This may be the consequence of a slower formation of complex A due to lower U2 snRNA and, indirectly, U2 snRNP amounts. Alternatively, a reduced conversion rate of complex A into complex B and downstream structures could occur because of the observed tri-snRNP defects. In addition, we cannot exclude that the rate of some proof-reading mechanism that dissociates or degrades abnormal B or C complex assemblies is faster than that of full spliceosome formation, preventing the accumulation of early complexes.

Together, our results from glycerol gradient fractionation, immunoprecipitation and *in vitro* spliceosome assembly show that all *RP-PRPF* mutations included in this study delay spliceosome assembly, but may act through different molecular mechanisms. While *PRPF31* mutations likely affect tri-snRNP formation directly, *PRPF8* and *PRPF3* mutations could indirectly impair both U4/U6.U5 assembly and the catalytic activation of the spliceosome. However, in cell lines from patients, these defects did not lead to aberrant localization of RP-PRPF proteins and their interacting partners (Supplementary Material, Figs S6 and S7) or to spliceosome destabilization due to putative protein decay (Supplementary Material, Fig. S3), in contrast to what has been observed after exogenous overexpression of mutant PRPF31 protein in HeLa or PRPF3 in photoreceptor-derived murine cells (43,44). The observed defects are also less pronounced compared with the data obtained using thermo-sensitive (haploid) mutant yeast or siRNA-silenced cells (29,31,37), likely because patients are heterozygotes and carry one fully functional copy of RP-PRPF that prevents the complete block of the spliceosome.

Pre-mRNA splicing analyses in extracts from patients showed that the observed defects in spliceosome composition translated into a reduction in splicing activity. Although the splicing process itself was not abolished (as expected, since heterozygous *RP-PRPF* mutations are not lethal), its efficiency was reduced. This is probably a direct consequence of observed defects detected *in vitro* with extracts bearing *PRPF* mutations. While it is difficult to extrapolate these results to an *in vivo* context, it is plausible that *RP-PRPF* mutations can cause a systemic splicing defect in patients. In support of this view, we showed that 8.8% of the introns from naturally expressed genes (summarizing different assortments of splicing signals) displayed dramatic splicing problems in lymphoblasts from patients. This value may be even higher considering that our experimental setup did not take into consideration the counteracting effect of nonsense-mediated decay, a cellular sentinel eliminating many abnormally spliced transcripts. The mis-spliced transcripts identified in this study, selected mainly because of their intronic splicing motifs, are likely not directly involved in RP pathogenesis. However, they clearly indicate that cells with RP-PRPF mutations display transcript-specific defects, in agreement with data from yeast (45) and human cells (46). The nature of the signal, motif or structure that confers responsiveness to defective PRPF proteins remains for the moment unknown.

The analysis of AS in RP-PRPF cells identified alterations in splicing patterns in a subset of the transcripts analyzed. Although all of them seemed to be expressed in the retina according to online databases, it is difficult to find a direct link between these transcripts and RP. It is perhaps worth noting that mutations in the zebrafish homolog of *AXIN1* result in dwarfed or absent eye development (47). However, this ocular phenotype is clinically different from RP, and therefore this finding may have no particular meaning from a mechanistic point of view. The effects of PRPF8 depletion on ASEs were more pronounced compared with the partial RP-PRPF deficiencies displayed by heterozygous cell lines. When the beneficial effects of wild-type PRPF8 were removed, ~10% of the investigated transcripts displayed changes in AS pattern in at least four of the five cell lines depleted of PRPF8.

Although tri-snRNP is a constitutive splicing factor, reduction in its level or its composition may also impact AS. Direct effects on AS may occur because of the observed slowdown of specific U4/U6.U5-dependent steps of spliceosome assembly on competing pairs of splice sites. Similarly, it was demonstrated that mutations in the RNA portion of the constitutive splicing factor U1 snRNP can change its affinity for competing splice sites and alter splice site selection (48). Likewise, mutations in SMN, a protein component essential for the snRNP maturation machinery, change the stoichiometry of snRNAs and promote defects in the AS of numerous transcripts (23). Also, down-regulation of constitutive splicing factors U2AF65 and PUF60 in mammalian cells and core spliceosome components in *Drosophila* can alter the choice of alternative splice sites (49–51). There may, however, be alternate explanations. For example, altered tri-snRNP particles may elicit secondary defects in the expression of one or several splicing regulatory proteins. Secondary effects could also alter the expression of a factor unrelated to splicing that is involved in differential mRNA stability, thereby changing the relative proportion of different splice forms.

Remarkably, changes in AS patterns in RP-PRPF cells and upon PRPF8 knock-down also suggest that late steps of spliceosome function can reprogram splicing decisions. In agreement with this, the U5 snRNP-associated factors PRPF6 and USP39 have recently been shown to affect the splice site choice for several transcripts, including *Mcl1* (52).

Although patients with *RP-PRPF* mutations have splicing defects in their lymphoblasts and presumably in other tissues as well, they show disease only in the retina, likely because of a threshold effect determined by its high pre-mRNA

splicing activity. These mutations may affect many tissues at sub-pathological levels, or may not manifest their deleterious effects within a human lifetime, whereas retinal cells could undergo cell death due to an increased accumulation of aberrant mRNAs produced through impaired constitutive and/or AS. Another model, which is not incompatible with the previous one, would rely on mechanisms involving selective mis-splicing of one or a few RP genes (53,54), although specific studies investigating this possibility have not analyzed mRNA from non-ocular tissues (55,56), and recent results have shown that processing of two transcripts important for photoreceptor function in human cells is not affected by RP-PRPF mutations (57). At the moment, our data cannot unambiguously favor one model over the other, and the precise mechanisms by which these defects lead to photoreceptor cell death remain to be clarified.

In conclusion, autosomal dominant RP caused by mutations in *PRPF* genes seems to be a generalized splicing disease that may more dramatically affect a subset of pre-mRNAs. In agreement with the observation that patients do not suffer from syndromic symptoms and appear to have a normal lifespan (58), functional splicing defects are globally mild compared with lethal *PRPF* knockouts in yeast and mammalian cells. This picture is very similar to that recently shown for another tissue-specific and progressive disorder, spinal muscular atrophy, which is caused by the systemic deficiency of SMN, a protein that is essential for the biogenesis of snRNPs (23). Our results indicate that future treatment strategies for PRPF-linked RP should be aimed at correcting pre-mRNA splicing impairment.

MATERIALS AND METHODS

Patients and cell culture

This study involved human subjects and was carried out in accordance with the tenets of the Declaration of Helsinki and was approved by the IRBs of the Massachusetts Eye and Ear Infirmary, Harvard Medical School and University of Lausanne. We recruited 13 patients with dominant retinitis pigmentosa and mutations in *PRPF31* (59), *PRPF8* (60) or *PRPF3*, as well as control individuals (14251, 13167, 14419, 29459, 29460, 13577, 13491). All patients were clinically evaluated with an ophthalmologic examination including visual field testing and electroretinography. Dominant inheritance of the disease was inferred from family history and confirmed by the presence of two or more generations of affected relatives. Upon signature of an informed consent, these individuals donated 10–50 ml of blood, from which lymphoblast cells were obtained and cultured as described previously (54). Lymphoblasts from patient AG0293, previously clinically described (61), were purchased from the European Collection of Cell Cultures. Control cells GM10858 were bought from Coriell Cell Repository and cell lines H1, D1, K2 and E2 are from centre d'Etude du polymarphisme humain collection (62).

The prostate cancer cell line PC-3 was grown in HAM's F12, the breast cancer cells MCF-7 in Minimum Essential Medium Eagle's, MBA-MB-231 cells in dulbecco's modified eagle's medium (DMEM), the ovarian cancer cell line OVCAR-3 in RPMI 1640 and the SKOV3 cell line in a 50/50 mix of DMEM/F12. All media were supplemented with 10% fetal bovine serum (Wisent) (except OVCAR-3, which contained 20%) and 2 mM L-glutamine.

Nuclear extracts

Lymphoblast cells in exponential growth (1×10^6 cells/ml) were collected and nuclear extracts prepared as described previously (63,64). At least four different extracts were produced for each cell line, starting from independent cultures. All extracts yielded reproducible results in all tests reported. Splicing-competent HeLa cell nuclear extracts were purchased from Cilbiotech.

Immunoprecipitation and glycerol gradient fractionation

Nuclear extracts (150 μg each) were incubated overnight at 4°C with 20 μl Protein G-Dynabeads (Invitrogen) coupled to anti-Sm antibodies (Thermo Scientific). The beads were washed six times with 1 ml of 20 mM Tris–HCl pH 7.4, 150 mM NaCl, 2.5 mM $MgCl_2$, 0.05% Nonidet-P40 and 0.5 mM dithiothreitol (DTT). Bound material was eluted with 2× SDS sample buffer, proteins separated by 8% sodium dodecyl sulfate polyacrylamide gel electrophoresis (SDS-PAGE), transferred to nitrocellulose and visualized by western blotting.

Glycerol gradient fractionation was performed as described by Makarova *et al*. (31).

Northern blotting

Total RNA from human tissues (8 μg each, see below) or RNA from glycerol gradient fractions were resolved in 10% polyacrylamide/8.3 M urea gels, transferred to nylon membranes and hybridized with major (65) and minor snRNA probes (66,67). Plasmids encoding the major and minor probes were kindly provided by Prof. Angela Krämer and Prof. Joan A. Steitz, respectively. All plasmids were linearized according to the references, and probes were made by *in vitro* transcription in the presence of 25 U SP6 RNA-polymerase (U4 and U5 snRNA probes), or 25 U T7 RNA-polymerase for the other probes (both from Promega), and 50 μCi α-^{32}P-UTP for 1 h at 37°C, according to the protocol supplied with the polymerases. The reactions were phenol/chloroform extracted, and the RNA probes were precipitated with ethanol and resuspended in RNase-free water. Hybridization was performed as described (65).

Western blotting

Nuclear extracts (20 μg per sample), glycerol gradient fractions or immunoprecipitated proteins were separated by 8% SDS–PAGE, and proteins were transferred to a nitrocellulose membrane and blotted as previously described (68). The following antibodies were used; primary antibodies: rabbit anti-PRPF31 (26), rabbit and mouse anti-PRPF8 (Santa Cruz Biotechnology), rabbit anti-PRPF3 (ProteinTech Group), mouse anti-PRPF3 (Abnova), rabbit anti-PRPF6 (Santa Cruz Biotechnology), rabbit anti-PRPF4 (ProteinTech Group),

mouse anti-PRPF4 (Abnova), goat anti-hBrr2 (Santa Cruz Biotechnology), rabbit anti-hSnu114 (Novus Biologicals), rabbit anti-SF3a60 (69), mouse anti-SF3a66 (70), rabbit anti-SF3a120 (71) and mouse anti-actin B (Sigma); secondary antibodies: goat anti-rabbit-horseradish peroxidase (HRP) (Jackson ImmunoResearch Laboratories), swine anti-rabbit-HRP, goat anti-mouse-HRP and rabbit anti-goat-HRP (all from Dako).

Densitometry and *in silico* analyses

Densitometry measurements of western blot signals were performed with the ImageJ 1.410 software (NIH), and quantification of northern blots was achieved either by the use of Molecular Imager FX and the QualityOne-4.6.3 software (BioRad), or ImageJ. Experimental uncertainty was expressed as standard deviations of the values obtained, or as standard errors. The analysis of 5′-ss, 3′-ss, BPS and poly-Py tract was obtained either via the alternative splicing database (ASD) workbench web interface (European Bioinformatics Institute) or by retrieving pre-computed scores form the ASD web site (72). Gene expression analysis in 31 human tissues was performed on the data set defined by Dezso *et al*. (20) for a subset of 2255 spliced housekeeping genes. For a given gene, the expression was computed as the average value over three tissue replicates. The 'gene expression score' for each tissue represents a cumulative count of occurrences for which a given sequence was maximally expressed and spliced in that tissue. For example, a tissue ranking first for the expression of n genes out of 2255 would have a gene expression score equal to n.

In vitro spliceosome assembly and splicing

RNA1 (Supplementary Material, Fig. S4A) is derived from the adenovirus *Major Late* transcription unit and was described previously (21). A deletion mutant of *RNA1* lacking the 5′-ss (Supplementary Material, Fig. S4B) was derived from the original plasmid; it contains 87 nucleotides upstream of the 3′-ss of intron 1 and 35 nucleotides of exon 2, up to the *Sca*I site. Both plasmids, kindly provided by Prof. Angela Krämer, were linearized with *Sca*I and used as templates for *in vitro* transcription with T3 RNA polymerase (Promega) in the presence of 50 μCi of α-^{32}P-UTP and 2 mM $m^7G(5')ppp(5')G$ for 1 h at 37°C, according to the instructions supplied with the polymerase. Following transcription, template DNA was digested with 2 U of RNase-free DNase for 15 min at 37°C, the reactions were phenol/chloroform extracted, precipitated with ethanol and RNA resuspended in RNA sample loading buffer. Samples were loaded on 10% polyacrylamide/8.3 M urea gels, and relevant bands were excised, eluted and resuspended in RNase-free water.

Splicing complexes were assembled on *RNA1* or its mutant version (20 000 cpm/reaction of radiolabeled RNA) with 70 μg of nuclear extract in the presence of 2 mM ATP, 10 mM creatinine phosphate, 3 mM $MgCl_2$, 20 U of RNasin Plus, 1 μg of tRNA, 10 mM Hepes-KOH pH 7.9, 50 mM KCl, 10% (V/V) glycerol, 0.1 mM ethylenediaminetetraacetic acid (EDTA) and 0.25 mM DTT. The reactions were incubated for 5, 10, 15, 30, 60 or 120 min at 30°C and terminated by the addition of heparin to a final concentration of 200 μg/ml and incubation at room temperature for 10 min. Complexes were resolved by native PAGE (concentrations indicated in the figure legend) according to electrophoresis conditions described previously (22), and visualized by autoradiography.

In vitro splicing reactions were performed with *RNA1*, as described above. Instead of adding heparin, reactions were treated with 4 μg of proteinase K in the presence of 2% sarcosyl, 100 mM Tris–HCl pH 7.5, 20 mM EDTA, and 20 U of RNasin plus for 15 min at 65°C. Splicing products were phenol/chloroform extracted, precipitated with ethanol, resuspended in RNA sample loading buffer, resolved in 8% polyacrylamide/8.3 M urea gels and visualized by autoradiography.

RNA samples and non-quantitative RT–PCR

Total RNA samples from cell lines were prepared by using 10×10^6cells and the RNeasy Mini kit (Qiagen), according to the manufacturer's instructions. RNAs from human retina, brain, heart, testis and skeletal muscle were purchased from Clontech; they represent pooled samples extracted from different subjects and were described previously (73). cDNA was made from these samples with oligo-dT primer, in the presence or absence (negative control) of reverse transcriptase as described (73). Non-quantitative RT–PCRs were performed with the Expand High Fidelity kit (Roche) with primers listed in Table S4 and cycling conditions adapted to the expression level of each transcript. Identity of each PCR product was confirmed by direct DNA sequencing.

siRNAs and qPCR

The siRNAs used for knocking down PRPF8 were purchased from IDT and their sequences were GAGAUAGGAGG CAUUUCAATT for si1 and CGCCGAGAAAAAAGA-GAUATT for si2. siRNAs were transfected into cells at a concentration of 100 nM using Lipofectamine 2000 (Invitrogen). RNA was extracted from mock-transfected and siRNA-transfected cells 96 h post-transfection. To assess the knockdown efficiency, we conducted quantitative real-time RT–PCR assays using SyberGreen (Applied Biosystems). Aldolase A (RTPrimerDB ID: 915) was used as the housekeeping gene on the same samples. A total of 200 ng of RNA measured for integrity (using the Agilent Bioanalyzer) and quantification (using the Thermo Scientific NanoDrop) was reverse transcribed using random hexamers (Roche) with Transcriptor Reverse transcriptase (Roche) in a final volume of 20 μl. Ten nanograms of cDNA were used for the quantification in the presence of the specific primers at 0.2 μM in a 10 μl reaction in triplicates. Reactions were carried out in the ABI 7500 qPCR (Applied Biosystems) or Eppendorf Realplex. A first cycle of 10 min at 95°C was followed by 40 cycles of 15 s at 94°C, 20 s at 55°C and 20 s at 68°C.

Splicing assays

A set of 96 AS units from various apoptotic and cancer-related genes were selected from the AceView database. Sets of primers mapping in the exons flanking the ASEs

were designed using Primer3 with default parameters. Primers were designed to cover alternatively spliced regions such that two distinct splice products of sizes ranging between 100 and 700 bp could be amplified. Our analysis considered only ASEs annotated in public databases such as NCBI, Ensembl and Aceview. For the global analysis of splice isoforms in cancer cell lines, total RNA was extracted using TRIzol and quantitated using the Bioanalyzer station (Agilent Inc.). A total of 2 μg of RNA was reverse transcribed using a mix of random hexamers and the Transcriptor Reverse transcriptase (Roche) in a final volume of 20 μl. Twenty nanograms of cDNA were amplified with 0.2 U/10 μl of HotStarTaq DNA Polymerase (Qiagen) in the buffer provided by the manufacturer, without extra $MgCl_2$ and in the presence of the specific primers (IDT) for each splicing unit at 400 nM and dNTPs. The list of units, oligos and expected size of RT–PCR products were reported previously (25). Reactions were carried out in the GeneAmp PCR system 9700 (Applied Biosystems). A first cycle of 15 min at 95°C was followed by 35 cycles of 30 s at 94°C, 30 s at 55°C and 1 min at 72°C. The reaction was ended with an extension step of 10 min at 72°C. Visualization and analysis of amplified products were performed using the LabChip HT™ DNA assay on an LC-90 automated microfluidic station (Caliper) (74).

To assess the significance of our results, we used a statistical approach tailored for the analysis of genomic data that produces a *q*-value (75), with a false discovery rate threshold of 0.15, indicating that only 15% of the results judged to be significant could represent false positive signals. In our case, this would correspond to less than one hit.

Immunostaining and fluorescence microscopy

Lymphoblasts were grown on top of cover slips coated with poly-L-lysine, fixed with −20°C methanol for 5 min and subsequently washed three times with 1xPBS. The following antibodies were used; primary antibodies: rabbit anti-PRPF31 (31), rabbit anti-PRPF8 (Santa Cruz Biotechnology), mouse anti-SC35 (Sigma) and mouse anti-coilin (Sigma); secondary antibodies: Texas Red-conjugated donkey anti-rabbit and fluorescein (FITC) conjugated donkey anti-mouse (all from Jackson ImmunoResearch Laboratories). All antibodies were incubated for 30 min at room temperature, with each incubation step followed by washing steps (five times for 5 min); all incubation and washing steps were done in 1xPBS containing 0.2% Nonidet-P40. Cells were mounted in Vectashield mounting media (Vector Laboratories) and examined using a Leica SP5 confocal microscope equipped with LAS 6000 AF software (Leica) and HCX PLAN APO 63x/1.40-0.60 NA/oil immersion lambdaBL objective. All images were recorded sequentially for Hoechst, FITC and Texas red emissions.

SUPPLEMENTARY MATERIAL

Supplementary Material is available at *HMG* online.

ACKNOWLEDGEMENTS

We thank M. Durand, E. Lapointe and S. Couture for technical assistance; A. Krämer, J.A. Steitz, R. Lührmann and C.L. Will for the provided material; A. Krämer and J.S. Beckmann for discussions and A. Title, P. Zavad'akova, R. Chrast, T. Abbas-Terki and A. Krämer for critical reading of the manuscript. We are also grateful to the Department of Biochemistry at University of Lausanne for the infrastructure for large-scale cell culturing.

Conflict of Interest statement. None declared.

FUNDING

This work was supported by the Swiss National Science Foundation [grants PMPDA-114446 from the Marie Heim-Vögtlin Programme (to G.T.) and grant 320000-121929 (to C.R.)]; the National Institutes of Health (grants EY00169 and P30-EY014104); The Foundation Fighting Blindness USA (to E.L.B.); by Research to Prevent Blindness (HMS, Department of Ophthalmology, Unrestricted Grant) and by the Canadian Institute of Health Research (to B.C.). S.A.E. is Chercheur National du FRSQ. B.C. is the Canada Research Chair in Functional Genomics.

REFERENCES

1. Vithana, E.N., Abu-Safieh, L., Allen, M.J., Carey, A., Papaioannou, M., Chakarova, C., Al-Maghtheh, M., Ebenezer, N.D., Willis, C., Moore, A.T. *et al.* (2001) A human homolog of yeast pre-mRNA splicing gene, PRP31, underlies autosomal dominant retinitis pigmentosa on chromosome 19q13.4 (RP11). *Mol. Cell*, **8**, 375–381.
2. McKie, A.B., McHale, J.C., Keen, T.J., Tarttelin, E.E., Goliath, R., van Lith-Verhoeven, J.J., Greenberg, J., Ramesar, R.S., Hoyng, C.B., Cremers, F.P. *et al.* (2001) Mutations in the pre-mRNA splicing factor gene PRPC8 in autosomal dominant retinitis pigmentosa (RP13). *Hum. Mol. Genet.*, **10**, 1555–1562.
3. Chakarova, C.F., Hims, M.M., Bolz, H., Abu-Safieh, L., Patel, R.J., Papaioannou, M.G., Inglehearn, C.F., Keen, T.J., Willis, C., Moore, A.T. *et al.* (2002) Mutations in HPRP3, a third member of pre-mRNA splicing factor genes, implicated in autosomal dominant retinitis pigmentosa. *Hum. Mol. Genet.*, **11**, 87–92.
4. Berson, E.L. (1993) Retinitis pigmentosa. The Friedenwald Lecture. *Invest. Ophthalmol. Vis. Sci.*, **34**, 1659–1676.
5. Li, N., Mei, H., Macdonald, I.M., Jiao, X. and Hejtmancik, F. (2009) Mutations in ASCC3L1 on chromosome 2q11.2 are associated with autosomal dominant retinitis pigmentosa in a Chinese Family. *Invest. Ophthalmol. Vis. Sci.*, **51**, 1036–1043.
6. Zhao, C., Bellur, D.L., Lu, S., Zhao, F., Grassi, M.A., Bowne, S.J., Sullivan, L.S., Daiger, S.P., Chen, L.J., Pang, C.P. *et al.* (2009) Autosomal-dominant retinitis pigmentosa caused by a mutation in SNRNP200, a gene required for unwinding of U4/U6 snRNAs. *Am. J. Hum. Genet.*, **85**, 617–627.
7. Keen, T.J., Hims, M.M., McKie, A.B., Moore, A.T., Doran, R.M., Mackey, D.A., Mansfield, D.C., Mueller, R.F., Bhattacharya, S.S., Bird, A.C. *et al.* (2002) Mutations in a protein target of the Pim-1 kinase associated with the RP9 form of autosomal dominant retinitis pigmentosa. *Eur. J. Hum. Genet.*, **10**, 245–249.
8. Maita, H., Kitaura, H., Keen, T.J., Inglehearn, C.F., Ariga, H. and Iguchi-Ariga, S.M. (2004) PAP-1, the mutated gene underlying the RP9 form of dominant retinitis pigmentosa, is a splicing factor. *Exp. Cell Res.*, **300**, 283–296.
9. Pan, Q., Shai, O., Lee, L.J., Frey, B.J. and Blencowe, B.J. (2008) Deep surveying of alternative splicing complexity in the human transcriptome by high-throughput sequencing. *Nat. Genet.*, **40**, 1413–1415.

10. Wang, E.T., Sandberg, R., Luo, S., Khrebtukova, I., Zhang, L., Mayr, C., Kingsmore, S.F., Schroth, G.P. and Burge, C.B. (2008) Alternative isoform regulation in human tissue transcriptomes. *Nature*, **456**, 470–476.
11. Wahl, M.C., Will, C.L. and Luhrmann, R. (2009) The spliceosome: design principles of a dynamic RNP machine. *Cell*, **136**, 701–718.
12. Patel, A.A. and Steitz, J.A. (2003) Splicing double: insights from the second spliceosome. *Nat. Rev. Mol. Cell Biol.*, **4**, 960–970.
13. Makarov, E., Makarova, O., Urlaub, H., Gentzel, M., Will, C., Wilm, M. and Luhrmann, R. (2002) Small nuclear ribonucleoprotein remodeling during catalytic activation of the spliceosome. *Science*, **298**, 2205–2208.
14. Liu, S., Rauhut, R., Vornlocher, H.P. and Luhrmann, R. (2006) The network of protein-protein interactions within the human U4/U6.U5 tri-snRNP. *RNA*, **12**, 1418–1430.
15. Deckert, J., Hartmuth, K., Boehringer, D., Behzadnia, N., Will, C.L., Kastner, B., Stark, H., Urlaub, H. and Luhrmann, R. (2006) Protein composition and electron microscopy structure of affinity-purified human spliceosomal B complexes isolated under physiological conditions. *Mol. Cell Biol.*, **26**, 5528–5543.
16. Bessonov, S., Anokhina, M., Will, C.L., Urlaub, H. and Luhrmann, R. (2008) Isolation of an active step I spliceosome and composition of its RNP core. *Nature*, **452**, 846–850.
17. Graziotto, J.J., Inglehearn, C.F., Pack, M.A. and Pierce, E.A. (2008) Decreased levels of the RNA splicing factor Prpf3 in mice and zebrafish do not cause photoreceptor degeneration. *Invest. Ophthalmol. Vis. Sci.*, **49**, 3830–3838.
18. Bujakowska, K.M., Maubaret, C., Chakarova, C.F., Tanimoto, N., Beck, S.C., Fahl, E., Humphries, M.M., Kenna, P., Makarov, E., Makarova, O. *et al.* (2009) Study of gene targeted mouse models of splicing factor gene Prpf31 implicated in human autosomal dominant retinitis pigmentosa (RP). *Invest. Ophthalmol. Vis. Sci.*, **50**, 5927–5933.
19. Graziotto, J., Farkas, M., Bujakowska, K.M., Deramaudt, B.M., Zhang, Q., Nandrot, E.F., Inglehearn, C.F., Bhattacharya, S.S. and Pierce, E.A. (2011) Three gene targeted mouse models of RNA splicing factor RP show late onset RPE and retinal degeneration. *Invest. Ophthalmol. Vis. Sci.*, **52**, 190–198.
20. Dezso, Z., Nikolsky, Y., Sviridov, E., Shi, W., Serebriyskaya, T., Dosymbekov, D., Bugrim, A., Rakhmatulin, E., Brennan, R.J., Guryanov, A. *et al.* (2008) A comprehensive functional analysis of tissue specificity of human gene expression. *BMC Biol.*, **6**, 49.
21. Arning, S., Grüter, P., Bilbe, G. and Krämer, A. (1996) Mammalian splicing factor SF1 is encoded by variant cDNAs and binds to RNA. *RNA*, **2**, 794–810.
22. Krämer, A. (1988) Pre-splicing complex formation requires two proteins and U2 snRNP. *Genes Dev.*, **2**, 1155–1167.
23. Zhang, Z., Lotti, F., Dittmar, K., Younis, I., Wan, L., Kasim, M. and Dreyfuss, G. (2008) SMN deficiency causes tissue-specific perturbations in the repertoire of snRNAs and widespread defects in splicing. *Cell*, **133**, 585–600.
24. Grainger, R.J. and Beggs, J.D. (2005) Prp8 protein: at the heart of the spliceosome. *RNA*, **11**, 533–557.
25. Venables, J.P., Koh, C.S., Froehlich, U., Lapointe, E., Couture, S., Inkel, L., Bramard, A., Paquet, E.R., Watier, V., Durand, M. *et al.* (2008) Multiple and specific mRNA processing targets for the major human hnRNP proteins. *Mol. Cell Biol.*, **28**, 6033–6043.
26. Rio Frio, T., Wade, N.M., Ransijn, A., Berson, E.L., Beckmann, J.S. and Rivolta, C. (2008) Premature termination codons in PRPF31 cause retinitis pigmentosa via haploinsufficiency due to nonsense-mediated mRNA decay. *J. Clin. Invest.*, **118**, 1519–1531.
27. Abu-Safieh, L., Vithana, E.N., Mantel, I., Holder, G.E., Pelosini, L., Bird, A.C. and Bhattacharya, S.S. (2006) A large deletion in the adRP gene PRPF31: evidence that haploinsufficiency is the cause of disease. *Mol. Vis.*, **12**, 384–388.
28. Sullivan, L.S., Bowne, S.J., Seaman, C.R., Blanton, S.H., Lewis, R.A., Heckenlively, J.R., Birch, D.G., Hughbanks-Wheaton, D. and Daiger, S.P. (2006) Genomic rearrangements of the PRPF31 gene account for 2.5% of autosomal dominant retinitis pigmentosa. *Invest. Ophthalmol. Vis. Sci.*, **47**, 4579–4588.
29. Schaffert, N., Hossbach, M., Heintzmann, R., Achsel, T. and Lührmann, R. (2004) RNAi knockdown of hPrp31 leads to an accumulation of U4/U6 di-snRNPs in Cajal bodies. *EMBO J.*, **23**, 3000–3009.
30. Nottrott, S., Urlaub, H. and Luhrmann, R. (2002) Hierarchical, clustered protein interactions with U4/U6 snRNA: a biochemical role for U4/U6 proteins. *EMBO J.*, **21**, 5527–5538.
31. Makarova, O.V., Makarov, E.M., Liu, S., Vornlocher, H.P. and Lührmann, R. (2002) Protein 61K, encoded by a gene (PRPF31) linked to autosomal dominant retinitis pigmentosa, is required for U4/U6.U5 tri-snRNP formation and pre-mRNA splicing. *EMBO J.*, **21**, 1148–1157.
32. Raghunathan, P.L. and Guthrie, C. (1998) RNA unwinding in U4/U6 snRNPs requires ATP hydrolysis and the DEIH- box splicing factor Brr2. *Curr. Biol.*, **8**, 847–855.
33. Laggerbauer, B., Achsel, T. and Lührmann, R. (1998) The human U5–200kD DEXH-box protein unwinds U4/U6 RNA duplices in vitro. *Proc. Natl Acad. Sci. USA*, **95**, 4188–4192.
34. Bartels, C., Klatt, C., Luhrmann, R. and Fabrizio, P. (2002) The ribosomal translocase homologue Snu114p is involved in unwinding U4/U6 RNA during activation of the spliceosome. *EMBO Rep.*, **3**, 875–880.
35. Small, E.C., Leggett, S.R., Winans, A.A. and Staley, J.P. (2006) The EF-G-like GTPase Snu114p regulates spliceosome dynamics mediated by Brr2p, a DExD/H box ATPase. *Mol. Cell*, **23**, 389–399.
36. Maeder, C., Kutach, A.K. and Guthrie, C. (2009) ATP-dependent unwinding of U4/U6 snRNAs by the Brr2 helicase requires the C terminus of Prp8. *Nat. Struct. Mol. Biol.*, **16**, 42–48.
37. Boon, K.L., Grainger, R.J., Ehsani, P., Barrass, J.D., Auchynnikava, T., Inglehearn, C.F. and Beggs, J.D. (2007) prp8 mutations that cause human retinitis pigmentosa lead to a U5 snRNP maturation defect in yeast. *Nat. Struct. Mol. Biol.*, **14**, 1077–1083.
38. Gonzalez-Santos, J.M., Wang, A., Jones, J., Ushida, C., Liu, J. and Hu, J. (2002) Central region of the human splicing factor Hprp3p interacts with Hprp4p. *J. Biol. Chem.*, **277**, 23764–23772.
39. Makarov, E.M., Makarova, O.V., Achsel, T. and Luhrmann, R. (2000) The human homologue of the yeast splicing factor prp6p contains multiple TPR elements and is stably associated with the U5 snRNP via protein-protein interactions. *J. Mol. Biol.*, **298**, 567–575.
40. Lutzelberger, M., Bottner, C.A., Schwelnus, W., Zock-Emmenthal, S., Razanau, A. and Kaufer, N.F. (2009) The N-terminus of Prp1 (Prp6/U5–102 K) is essential for spliceosome activation in vivo. *Nucleic Acids Res.*, **38**, 1610–1622.
41. Schneider, M., Hsiao, H.H., Will, C.L., Giet, R., Urlaub, H. and Luhrmann, R. (2010) Human PRP4 kinase is required for stable tri-snRNP association during spliceosomal B complex formation. *Nat. Struct. Mol. Biol.*, **17**, 216–221.
42. Ayadi, L., Miller, M. and Banroques, J. (1997) Mutations within the yeast U4/U6 snRNP protein Prp4 affect a late stage of spliceosome assembly. *RNA*, **3**, 197–209.
43. Comitato, A., Spampanato, C., Chakarova, C., Sanges, D., Bhattacharya, S.S. and Marigo, V. (2007) Mutations in splicing factor PRPF3, causing retinal degeneration, form detrimental aggregates in photoreceptor cells. *Hum. Mol. Genet.*, **16**, 1699–1707.
44. Deery, E.C., Vithana, E.N., Newbold, R.J., Gallon, V.A., Bhattacharya, S.S., Warren, M.J., Hunt, D.M. and Wilkie, S.E. (2002) Disease mechanism for retinitis pigmentosa (RP11) caused by mutations in the splicing factor gene PRPF31. *Hum. Mol. Genet.*, **11**, 3209–3219.
45. Ben-Yehuda, S., Russell, C.S., Dix, I., Beggs, J.D. and Kupiec, M. (2000) Extensive genetic interactions between PRP8 and PRP17/CDC40, two yeast genes involved in pre-mRNA splicing and cell cycle progression. *Genetics*, **154**, 61–71.
46. Ivings, L., Towns, K.V., Matin, M.A., Taylor, C., Ponchel, F., Grainger, R.J., Ramesar, R.S., Mackey, D.A. and Inglehearn, C.F. (2008) Evaluation of splicing efficiency in lymphoblastoid cell lines from patients with splicing-factor retinitis pigmentosa. *Mol. Vis.*, **14**, 2357–2366.
47. Heisenberg, C.P., Houart, C., Take-Uchi, M., Rauch, G.J., Young, N., Coutinho, P., Masai, I., Caneparo, L., Concha, M.L., Geisler, R. *et al.* (2001) A mutation in the Gsk3-binding domain of zebrafish Masterblind/Axin1 leads to a fate transformation of telencephalon and eyes to diencephalon. *Genes Dev.*, **15**, 1427–1434.
48. Yuo, C.-Y. and Weiner, A.M. (1989) A U1 small nuclear ribonucleoprotein particle with altered specificity induces alternative splicing of an adenovirus E1A mRNA precursor. *Mol. Cell Biol.*, **9**, 3429–3437.
49. Hastings, M.L., Allemand, E., Duelli, D.M., Myers, M.P. and Krainer, A.R. (2007) Control of pre-mRNA splicing by the general splicing factors PUF60 and U2AF(65). *PLoS ONE*, **2**, e538.
50. Warf, M.B., Diegel, J.V., von Hippel, P.H. and Berglund, J.A. (2009) The protein factors MBNL1 and U2AF65 bind alternative RNA structures to regulate splicing. *Proc. Natl Acad. Sci. USA*, **106**, 9203–9208.

51. Park, J.W., Parisky, K., Celotto, A.M., Reenan, R.A. and Graveley, B.R. (2004) From the cover: identification of alternative splicing regulators by RNA interference in Drosophila. *Proc. Natl Acad. Sci. USA*, **101**, 15974–15979.
52. Moore, M.J., Wang, Q., Kennedy, C.J. and Silver, P.A. (2010) An alternative splicing network links cell-cycle control to apoptosis. *Cell*, **142**, 625–636.
53. Baehr, W. and Chen, C.K. (2001) RP11 and RP13: unexpected gene loci. *Trends Mol. Med.*, **7**, 484–486.
54. Rivolta, C., McGee, T.L., Rio Frio, T., Jensen, R.V., Berson, E.L. and Dryja, T.P. (2006) Variation in retinitis pigmentosa-11 (*PRPF31* or *RP11*) gene expression between symptomatic and asymptomatic patients with dominant *RP11* mutations. *Hum. Mutat.*, **27**, 644–653.
55. Yuan, L., Kawada, M., Havlioglu, N., Tang, H. and Wu, J.Y. (2005) Mutations in PRPF31 inhibit pre-mRNA splicing of rhodopsin gene and cause apoptosis of retinal cells. *J. Neurosci.*, **25**, 748–757.
56. Linder, B., Dill, H., Hirmer, A., Brocher, J., Lee, G.P., Mathavan, S., Bolz, H.J., Winkler, C., Laggerbauer, B. and Fischer, U. (2011) Systemic splicing factor deficiency causes tissue-specific defects: a zebrafish model for retinitis pigmentosa. *Hum. Mol. Genet.*, **20**, 368–377.
57. Wilkie, S.E., Vaclavik, V., Wu, H., Bujakowska, K., Chakarova, C.F., Bhattacharya, S.S., Warren, M.J. and Hunt, D.M. (2008) Disease mechanism for retinitis pigmentosa (RP11) caused by missense mutations in the splicing factor gene PRPF31. *Mol. Vis.*, **14**, 683–690.
58. Berson, E.L., Gouras, P., Gunkel, R.D. and Myrianthopoulos, N.C. (1969) Dominant retinitis pigmentosa with reduced penetrance. *Arch. Ophthalmol.*, **81**, 226–234.
59. McGee, T.L., Berson, E.L. and Dryja, T.P. (2002) Identification of novel mutations in the PRPF31 gene (RP11) in patients with autosomal dominant retinitis pigmentosa with reduced penetrance. *Invest. Ophthalmol. Vis. Sci.*, **43**, E-Abstract 792.
60. De Erkenez, A.C., Berson, E.L. and Dryja, T.P. (2002) Novel mutations in the PRPC8 gene, encoding a Pre-mRNA splicing factor in patients with autosomal dominant retinitis pigmentosa. *Invest. Ophthalmol. Vis. Sci.*, **43**, E-Abstract 791.
61. Moore, A.T., Fitzke, F., Jay, M., Arden, G.B., Inglehearn, C.F., Keen, T.J., Bhattacharya, S.S. and Bird, A.C. (1993) Autosomal dominant retinitis pigmentosa with apparent incomplete penetrance: a clinical, electrophysiological, psychophysical, and molecular genetic study. *Br. J. Ophthalmol.*, **77**, 473–479.
62. Dausset, J., Cann, H., Cohen, D., Lathrop, M., Lalouel, J.M. and White, R. (1990) Centre d'etude du polymorphisme humain (CEPH): collaborative genetic mapping of the human genome. *Genomics*, **6**, 575–577.
63. Dignam, J.D., Lebovitz, R.M. and Roeder, R.G. (1983) Accurate transcription initiation by RNA polymerase II in a soluble extract from isolated mammalian nuclei. *Nucleic Acids Res.*, **11**, 1475–1489.
64. Krämer, A. and Keller, W. (1990) In Abelson, J.N. (ed.), *Methods Enzymol*. Academic Press, New York, Vol. 181, pp. 3–19.
65. Utans, U., Behrens, S.-E., Lührmann, R., Kole, R. and Krämer, A. (1992) A splicing factor that is inactivated during in vivo heat shock is functionally equivalent to the [U4/U6.U5] triple snRNP-specific proteins. *Genes Dev.*, **6**, 631–641.
66. Wassarman, K.M. and Steitz, J.A. (1992) The low-abundance U11 and U12 small nuclear ribonucleoproteins (snRNPs) interact to form a two-snRNP complex. *Mol. Cell Biol.*, **12**, 1276–1285.
67. Tarn, W.Y. and Steitz, J.A. (1996) Highly diverged U4 and U6 small nuclear RNAs required for splicing rare AT-AC introns. *Science*, **273**, 1824–1832.
68. Tanackovic, G. and Kramer, A. (2005) Human splicing factor SF3a, but not SF1, is essential for pre-mRNA splicing in vivo. *Mol. Biol. Cell*, **16**, 1366–1377.
69. Krämer, A., Legrain, P., Mulhauser, F., Gröning, K., Brosi, R. and Bilbe, G. (1994) Splicing factor SF3a60 is the mammalian homologue of PRP9 of *S. cerevisiae*: the conserved zinc finger-like motif is functionally exchangeable in vivo. *Nucleic Acids Res.*, **22**, 5223–5228.
70. Brosi, R., Hauri, H.P. and Krämer, A. (1993) Separation of splicing factor SF3 into two components and purification of SF3a activity. *J. Biol. Chem.*, **268**, 17640–17646.
71. Krämer, A., Mulhauser, F., Wersig, C., Gröning, K. and Bilbe, G. (1995) Mammalian splicing factor SF3a120 represents a new member of the SURP family of proteins and is homologous to the essential splicing factor PRP21p of *S. cerevisiae*. *RNA*, **1**, 260–272.
72. Thanaraj, T.A., Stamm, S., Clark, F., Riethoven, J.J., Le Texier, V. and Muilu, J. (2004) ASD: the alternative splicing database. *Nucleic Acids Res.*, **32**, D64–D69.
73. Tanackovic, G. and Rivolta, C. (2009) PRPF31 alternative splicing and expression in human retina. *Ophthalmic Genet.*, **30**, 76–83.
74. Klinck, R., Bramard, A., Inkel, L., Dufresne-Martin, G., Gervais-Bird, J., Madden, R., Paquet, E.R., Koh, C., Venables, J.P., Prinos, P. *et al.* (2008) Multiple alternative splicing markers for ovarian cancer. *Cancer Res.*, **68**, 657–663.
75. Storey, J.D. and Tibshirani, R. (2003) Statistical significance for genomewide studies. *Proc. Natl Acad. Sci. USA*, **100**, 9440–9445.